Multi-phase field simulation of grain growth in multiple phase transformations of a binary alloy*

Li Feng(冯力)[1,2,†], Beibei Jia(贾北北)[1], Changsheng Zhu(朱昶胜)[2], Guosheng An(安国升)[1,2], Rongzhen Xiao(肖荣振)[1,2], and Xiaojing Feng(冯小静)[1]

[1] College of Materials Science and Engineering, Lanzhou University of Technology, Lanzhou 730050, China
[2] State Key Laboratory of Advanced Processing and Recycling of Non-ferrous Metals, Lanzhou 730050, China

(Received 5 March 2017; revised manuscript received 27 April 2017; published online 20 June 2017)

This work establishes a temperature-controlled sequence function, and a new multi-phase-field model, for liquid–solid–solid multi-phase transformation by coupling the liquid–solid phase transformation model with the solid–solid phase transformation model. Taking an Fe–C alloy as an example, the continuous evolution of a multi-phase transformation is simulated by using this new model. In addition, the growth of grains affected by the grain orientation of the parent phase (generated in liquid–solid phase transformation) in the solid–solid phase transformation is studied. The results show that the morphology of ferrite grains which nucleate at the boundaries of the austenite grains is influenced by the orientation of the parent austenite grains. The growth rate of ferrite grains which nucleate at small-angle austenite grain boundaries is faster than those that nucleate at large-angle austenite grain boundaries. The difference of the growth rate of ferrites grains in different parent phase that nucleate at large-angle austenite grain boundaries, on both sides of the boundaries, is greater than that of ferrites nucleating at small-angle austenite grain boundaries.

Keywords: multi-phase transformation, microstructure, multi-phase-field method, grain orientation

PACS: 05.45.Pq, 05.70.Fh, 61.66.Dk, 64.75.Gh **DOI:** 10.1088/1674-1056/26/8/080504

1. Introduction

The observation and quantitative characterisation of the microstructure of steel and iron materials is both a focus, and a difficulty, in the field of materials science and engineering.[1] The microstructure of a material determines its mechanical properties, while phase transformation parameters control the morphology and affect the material properties.[2,3] The formation of most iron and steel materials involves multiple phase transformations; however, during the forming of iron and steel materials, many parameters need to be controlled, accompanied by the many difficulties caused by their opacity, size, and the high temperatures involved. For this reason, it is not possible to observe, and quantitatively characterize, the evolution of microstructure in phase transformation by experimental methods. With the development of computer technology, numerical simulation provides a new method for researchers. By simulating the formation and evolution of microstructure at the grain size scale, quantitative relationships between the parameters and final microstructure are obtained,[4,5] and applied in actual production to optimize the process and thereby improve industrial output. In materials science and related areas, the phase field method is widely used as a powerful computational method to simulate the formation of complex microstructures during solidification and solid-state phase transformation of metals and alloys. The phase field method does not need to keep track of the location of interfaces and overcomes the disadvantages of MC and CA methods. With these unique advantages in material microstructure simulation, the phase field method has therefore been widely used in iron and steel material microstructure research.[6–21]

However, the phase field simulation of the microstructural evolution during the phase transformation of alloys mainly focuses on the simulation of the single phase transformation process.[6–10,14–22] For example, Feng[8,9] simulated the dendritic growth process of multiple grains during isothermal solidification, Huang,[14] Loginoval,[15] and Mecozzi[16] simulated γ–α phase transformation by the phase field model. As a matter of fact, alloy materials generally have to undergo multiple phase transformations including solidification transformation and solid-state transformation during their formation. For example, the formation of Fe–C alloy usually entails phase transformation from liquid state to an austenite phase (the solidification process) together with the later phase transformation from austenite to ferrite[14–22] or from austenite to pearlite (the solid state phase transformation). Phase field simulation of a single phase transformation is not able to characterise the continuous evolution of alloy microstructures including solidification and solid state phase transformation and the influences of the former on the latter. Simulation of multi-phase transformation can not only predict the characteristics of the microstructure of grains but can also control and optimise the microstructure and mechanical proper-

*Project supported by the National Natural Science Foundation of China (Grant Nos. 51661020, 11504149, and 11364024).
†Corresponding author. E-mail: fenglils@lut.cn
© 2017 Chinese Physical Society and IOP Publishing Ltd

ties of metal materials.[23,24] To simulate better the evolution of alloy microstructure during the forming process using the phase field method, and therefore control the microstructure and macroscopic properties of materials, we need to simulate multi-phase transformations of the alloy in solidification, and the solid state transformation, by using a multi-phase-field method.

In this work, a new multi-phase field model is established for liquid–solid–solid multiple phase transformation by coupling the solidification transformation model with a solid state phase transformation model. Taking an Fe–C binary alloy as an example, the authors analyze the continuous evolution mechanism of microstructure in the formation of the alloy and the influences of the previous solidification transformation on the later solid state transformation.

2. Multi-phase-field model

2.1. Model equation

2.1.1. Phase field equation

The authors establish a sequence function which is controlled by temperature. Based on the multi-phase field model for a single phase transformation,[25] the phase field equation is re-characterised with the aid of that sequential function[26]

$$\frac{\partial \phi}{\partial t} = \sum_{\alpha \neq \beta}^{m} K_{\alpha\beta} \cdot \frac{2}{n} \sum_{j \neq i}^{n} S_{ij} M_{ij} \left(\frac{\delta F}{\delta \phi_i} - \frac{\delta F}{\delta \phi_j} \right), \tag{1}$$

where ϕ_i and ϕ_j are the phase field parameters of different phases, representing different phase structures, S_{ij} is the space step function, M_{ij} is the interface migration rate, F represents the system free energy, and K is the time sequence function. K is similar to the definition of the space step function S, and is a function relating to system temperature and free energy. In addition, m is the number of phase transformations undergone in the process. The subscripts i and j respectively represent the new phase and parent phase in the solidification phase transformation and solid state transformation while the subscripts α and β respectively represent solidification phase transformation and solid-state phase transformation in multiple phase transformations. The definition of the sequence function K is as follows:

$$K_\alpha(T_t^x, f^i) = 1, \quad (T_t^x \leq T_i^e), \tag{2}$$

$$K_\alpha(T_t^x, f^i) = 0, \quad (T_t^x > T_i^e), \tag{3}$$

where, T^x represents the system temperature, and T^e represents the temperature at the beginning of the phase transformation.

Both solidification phase transformation and austenite-ferrite phase transformation in an Fe–C alloy are nucleation-growth induced phase transformations,[27] so they have consistent structure implicit in their multi-phase-field governing equations. However, the volume change in liquid–solid phase transformation is unable to change the free energy at the interface, but the volume change in a solid–solid phase transformation will lead to a change in the free energy of the system. So they have different definitions of free energy, the specific definitions are as follows:

$$F = \int_{\Omega} f^{\mathrm{GB}} + f^{\mathrm{CH}} + f^{\mathrm{EL}} + f^{\mathrm{T}}, \tag{4}$$

where, f^{GB}, f^{CH}, and f^{EL} denote the interfacial, component, and elastic free energy densities, respectively; f^{T} represents free energy density relating to a specific temperature,[28] and

$$f^{\mathrm{GB}} = \sum_{i,j=1}^{N} \frac{4\sigma_{ij}}{\eta_{ij}} \left\{ \frac{\eta_{ij}^2}{\pi^2} \left| \nabla\phi_i \cdot \nabla\phi_j \right| + W_{ij} \right\}, \tag{5}$$

$$f^{\mathrm{CH}} = \sum_{i=1}^{N} \phi_i f^i(c_i), \tag{6}$$

$$f^{\mathrm{EL}} = \frac{1}{2}(\varepsilon^{ij} - \varepsilon^{*ij}) C^{ijkl} (\varepsilon^{kl} - \varepsilon^{*kl}), \tag{7}$$

$$f^{\mathrm{T}} = h(\phi_i) G_i^{\mathrm{reg}} + (1 - h(\phi)) G_j^{reg} + W g(\phi_i), \tag{8}$$

where, σ_{ij}, η_{ij}, W_{ij}, $f^i(c_i)$, C^{ijkl}, and ε represent the interfacial energy, interface thickness, potential-well function, component free energies of solute c in phase i, the effective elasticity matrix, and the phase-field gradient coefficient. In addition, G^{reg} denotes the Gibbs free energy, W is the double well potential, and $Wg(\phi)$ is the excess free energy. In the middle of this, $h(\phi) = \phi^3(6\phi^2 - 15\phi + 10)$, $\mathrm{g}(\phi) = \phi^2(\phi^2 - 2\phi + 1)$. To simplify the model, in this research the influence of the stress and strain fields is ignored in the composition of F. In this way, the free energy F changes to the form given by formula (9)

$$F = \int_{\Omega} f^{\mathrm{GB}} + f^{\mathrm{CH}} + f^{\mathrm{T}}. \tag{9}$$

2.1.2. Solute control equation

$$\begin{aligned} \frac{\partial c}{\partial t} &= \nabla \left[M_c \nabla \left(\frac{\delta F}{\delta C} \right) \right] = \nabla \left[\frac{D(c,\phi)}{\partial^2 f / \partial c^2} \nabla \left(\frac{\partial f}{\partial c} \right) \right] \\ &= \nabla \left[\frac{D(c,\phi)}{f_{cc}} \nabla f_c \right], \end{aligned} \tag{10}$$

where, $D(c,\phi)$ is the solute diffusion coefficient, and f_c and f_{cc} are the first- and second-order partial differential equations of free energy density

$$f_c(c,\phi) = \frac{\mathrm{d}f^i(c_i)}{\mathrm{d}c_i} = \frac{\mathrm{d}f^j(c_j)}{\mathrm{d}c_j}, \tag{11}$$

$$f_{cc}(c,\phi) = \frac{f_{cc}^i(c_i) \cdot f_{cc}^j(c_j)}{[1 - h(\phi)] f_{cc}^j(c_j) + h(\phi) f_{cc}^i(c_i)}, \tag{12}$$

where, the subscripts i and j respectively represent the newly generated phase and parent phase in the solidification phase transformation or solid state transformation.

2.1.3. Temperature control equation

$$\frac{\partial T}{\partial t} = D_t \cdot \nabla^2 T - \frac{L(1-c)+L'c}{C_p} h'(\phi)\frac{\partial \phi}{\partial t} - \frac{(L-L')}{C_p} \times \left[1-h'(\phi)\right]\frac{\partial c}{\partial t}, \tag{13}$$

where, D_t, C_p, L, L', T, and c represent the heat diffusion coefficient, specific heat, latent heat of the solvent, latent heat of the solute, temperature, and concentration of the solute elements.[29]

2.2. The grain nucleation of solid-state phase transformation in multiple phase transformations

It is found that there are two nucleation mechanisms in the formation process of crystal nucleus: spontaneous homogeneous nucleation and non-spontaneous heterogeneous nucleation. In this work, the authors adopt non-spontaneous, and spontaneous, nucleation for the solidification transformation and the solid-state phase transformation. In the solid state phase transformation, the free energy of the system is[27]

$$\Delta G = -V_\beta(\Delta G_{\rm V} - \Delta G_\varepsilon) + A_\beta \sigma_{\alpha\beta} - \Delta G_{\rm d}, \tag{14}$$

where, V_β, $\Delta G_{\rm V}$, ΔG_ε, A_β, $\sigma_{\alpha\beta}$, and $\Delta G_{\rm d}$ are the volume of the β-phase, free energy change per unit volume of β-phase, the strain energy per unit volume, the area of the phase interface, the interfacial energy per unit volume, and the energy released at defects during nucleation. To simplify the model, the effect of strain energy on free energy is ignored; the nucleation site of a grain is calculated by its free energy. The nucleation rate of the solid-state phase transformation follows a Gaussian distribution, the number of solid cores can meet a certain relationship given a certain degree of cooling, and the nucleation density is calculated by using Eq. (15).

$$I = R \cdot N^* = R\left[N_0 \cdot \exp\left(-\frac{\Delta G^*}{k_{\rm B}T}\right)\right] = I_o \cdot \exp\left(-\frac{\Delta G^*}{k_{\rm B}T}\right), \tag{15}$$

where N^* and ΔG^* represent the critical nucleation rate and critical free energy barrier of nucleation, N_0 is the number of atoms per unit volume, $k_{\rm B}$ is the Boltzmann constant, and T is the absolute thermodynamic temperature.[11]

2.3. Phase field parameters and physical parameters

2.3.1. Phase field parameters

When liquid–solid phase transformation, the phase field equation is

$$\frac{\partial \phi}{\partial t} = M_\alpha\left(\varepsilon(\theta)^2\nabla^2\phi + \frac{\partial}{\partial x}\left(|\nabla\phi|^2\varepsilon(\theta)\frac{\partial\varepsilon(\theta)}{\partial(\phi_x)}\right) + \frac{\partial}{\partial y}\left(|\nabla\phi|^2\varepsilon(\theta)\frac{\partial\varepsilon(\theta)}{\partial(\phi_y)}\right) - f_\phi\right). \tag{16}$$

The expression of the migration rate M_α of the liquid–solid phase transformation is

$$M_\alpha^{-1} = \frac{\varepsilon_0^3}{\sigma\sqrt{2W}}\left(\frac{1}{D}\zeta\left(c_L^e, c_S^e\right)\right), \tag{17}$$

$$\varepsilon_0 = \sqrt{\frac{6\lambda\sigma}{2.2}}, \tag{18}$$

$$W = \frac{6.6\sigma}{\lambda}, \tag{19}$$

$$\zeta = \frac{RT}{V_m}(c_l^e - c_s^e)^2 \times \int_0^1 \frac{h(\phi)\left[1-h(\phi)\right]}{\left[1-h(\phi)\right]c_l^e\left(1-c_l^e\right)+h(\phi)\,c_s^e\left(1-c_s^e\right)} \cdot \frac{{\rm d}\phi}{\phi\,(1-\phi)}. \tag{20}$$

With solid–solid phase transformation, the phase field equation is

$$\frac{\partial \phi}{\partial {\rm t}} = M_\beta\left(K_\phi\nabla^2\phi + p'(\phi)\left[f^\gamma(C^\gamma) - f^\alpha(C^\alpha) - \frac{\partial f^\gamma}{\partial C^\gamma}(C^\gamma - C^\alpha)\right] - \omega \cdot g'(\phi)\right). \tag{21}$$

The expression for the migration rate M_β of the solid–solid phase transformation is

$$M_\beta = K_M \cdot M_p \cdot \frac{2\sigma}{K_\phi}, \tag{22}$$

$$\sigma = \frac{\sqrt{K_\phi\,\omega}}{6\sqrt{2}}, \tag{23}$$

$$2\lambda = \alpha\sqrt{2}\frac{\sqrt{K_\phi}}{\sqrt{\omega}}, \tag{24}$$

$$M_p = 0.035 \cdot \exp\left(-\frac{17700}{T}\right), \tag{25}$$

$$K_M = -0.015T + 16.98, \tag{26}$$

where, K_M, M_p, λ, σ, and K_ϕ refer to the fitting coefficient, interface migration rate of the γ–α transformation in low-carbon steels, interface thickness, interface energy, and phase field parameters, respectively.

The growth of isotropic ferrite grains is very difficult to bring about in practical materials. In this work, the influence of anisotropy is considered on the basis of the solid-state phase transformation model established by Huang *et al.*[14] As the solidification transformation and solid-state transformation of Fe–C alloy are a continuous process, the former influences the latter. While growing in parent grains of different orientations, ferrite shows anisotropy due to the difference in its grain orien-

tation and the orientation of the parent phase. The anisotropy affects the interfacial energy and then acts on the phase field. In the solid-state phase transition model, the anisotropy of the interface is adjusted by the energy gradient coefficient. The total free energy F is the functional of the phase-field variables:

$$F = \int_V \left[m f_0(\phi_1, \phi_2, \ldots, \phi_n) + \frac{\kappa}{2} \sum_{i=1}^{n} (\nabla \phi_i)^2 \right] \mathrm{d}V. \quad (27)$$

The corresponding local functional is

$$f_0(\phi_1, \phi_2, \ldots, \phi_n) = \sum_{i=1}^{n} \left(\frac{\phi_i^4}{4} - \frac{\phi_i^2}{2} \right) + \sum_{i=1}^{n} \sum_{j>i}^{n} \gamma \phi_i^2 \phi_j^2 + \frac{1}{4}. \quad (28)$$

Considering the influence of orientation field on interfacial energy, gradient coefficient κ and phenomenological parameter γ are expressed as

$$\kappa(\theta) = \frac{\sum_{i=1}^{n} \sum_{j>i}^{n} \kappa_{i,j} \eta_i^2 \eta_j^2}{\sum_{i=1}^{n} \sum_{j>i}^{n} \eta_i^2 \eta_j^2}, \quad (29)$$

$$\gamma(\theta) = \frac{\sum_{i=1}^{n} \sum_{j>i}^{n} \gamma_{i,j} \eta_i^2 \eta_j^2}{\sum_{i=1}^{n} \sum_{j>i}^{n} \eta_i^2 \eta_j^2}, \quad (30)$$

where, $\kappa_{i,j}$ and $\gamma_{i,j}$ are obtained by using the following formulae:

$$\gamma_{i,j} = \frac{1}{2} \frac{4k(\theta_{i,j})m + 9\sigma(\theta_{i,j})^2}{4k(\theta_{i,j})m - 9\sigma(\theta_{i,j})^2}, \quad (31)$$

$$\kappa_{\alpha\gamma} = \kappa_0 \frac{\sigma(\theta_{\alpha\gamma})}{\sigma}, \quad (32)$$

where, $\theta_{\alpha\gamma}$ represents the orientation angle between the parent phase austenite grain and the newly-generated phase's ferrite grain. In any grain, $\kappa = \kappa_0 = 0.25 \times 10^{-6}$ J/m and $\gamma = \gamma_0 = 1.5$. In the interfacial region between grains with orientations i and j, $\kappa = \kappa_{i,j}$ and $\gamma = \gamma_{ij}$.[31]

2.3.2. Physical parameters of the material

The physical parameters of the material used in our calculations are summarized in the following Table 1.

Table 1. Physical parameters of the material.[10,14,22]

Parameter	C-0.6 wt%
Solid–liquid and solid–solid interface energy σ	0.204 J/m^2, 1 J/m^2
Liquid–solid phase transition and solid–solid phase transition temperature T	1780 K, 1048 K
Liquid phase and solid phase solute diffusion rates	2.0×10^{-8} 'm^2/s, 6.0×10^{-9} m^2/s
Diffusion rates of austenite and ferrite	6.0×10^{-9} m^2/s, 3.284×10^{-14} m^2/s
Gas constant R	8.314 J/(mol·K)
Latent heat L of solidification	277.5 J/g
Thermal diffusion coefficient	1.277×10^{-5} J/g
Specific heat capacity at constant pressure	0.75 J/(g·K)
Molar volume V	7.7×10^{-6} m^3/mol

3. Numerical calculation of the model

3.1. Disturbance

To simulate the random fluctuations upon disturbance during the real solidification process, a disturbance term needs to be added to the calculation. In this research, an artificial random disturbance is added in the phase field equation:

$$f\left[\frac{\partial \phi}{\partial t}\right] = \frac{\partial \phi}{\partial t} + 16 g(\phi) \chi \varpi, \quad (33)$$

where χ is a random number from -1 to 1, and ϖ is the time-dependent disturbance intensity factor associated.[8]

3.2. Initial boundary conditions

Assuming that the initial nucleation (solidification phase change) radius is R:

$$x^2 + y^2 \le R^2, \quad \phi = 1, \quad T = T_m - \Delta T, \quad (34)$$

$$x^2 + y^2 > R^2, \quad \phi = 0, \quad T = T_m - \Delta T, \quad (35)$$

where x and y represent the abscissa and ordinate, respectively, T is the dimension temperature, T_m is the melting point temperature, and ΔT is the degree of undercooling. The nuclei are randomly distributed in the simulated region, and the number of nuclei is less than the maximum number for nucleation. On the boundary of the simulated region, ϕ and c use the adiabatic boundary condition, i.e., a zero-Neumann boundary condition.

3.3. Numerical calculation method

The explicit finite difference method is used to solve Eqs. (1), (10), (13), and (14) at the same time step Δt. The time step Δt and the space step Δx (space step $\Delta x = \Delta y = 1 \times 10^{-8}$ m) need to meet the following stability condition:

$$\Delta t < \min\left\{ \Delta x^2/(4D_0), \Delta y^2/(4D_0) \right\}, \quad (36)$$

where Δt_1 and Δt_2 denote the time steps for the growth of austenite and ferrite, respectively. Δt_{11} is the time step used for calculation in the transition period from the previous liquid–solid transformation to the later solid–solid transformation, and D_0 is diffusion coefficient of the solute in the parent phase: the physical property parameters are summarised in Table 1.

The phase field simulation is affected by the interface thickness. In addition, the computational grids are very small, resulting in an onerous calculation workload. To ensure the

convergence and stability of all numerical calculations, small computational grids are needed to match such small time steps. In the process of alloy solidification and solid state transformation, the time required for phase transformation is not long, given sufficient phase-transformation driving force; however, Fe–C alloy has a large temperature difference from solidification to its solid-state phase transformation, and thus needs a long cooling time. If small time steps are used, it calls for remarkable amounts of calculations. To facilitate the simulation, the solute diffusion was controlled in the transition period from the end of the liquid–solid transformation to the beginning of the solid–solid transformation by using the solute diffusion equation given by Fick's law with time step Δt_{11} (Δt_{11} is the enlarged time step). In the transition period between the two phase transformations, no phase transformation occurs, so the spatial step size of the simulation is no longer affected by the interface thickness in the phase transformation. Larger time step sizes and larger space step sizes can then be used to calculate the solute diffusion and temperature diffusion. So Δt_{11} was used to simulate both solute, and temperature, diffusion in the transition period from the end of the liquid–solid transformation to the beginning of solid–solid transformation.

4. Results and analysis

4.1. Solidification phase transformation

A 1200×1200 two-dimensional grid is employed, the initial nuclei are set to a grid of 20 spheres, the coordinates of the nuclei are given randomly in the grid, but the number of nuclei is less than the value calculated by Eq. (15). The initial temperature is 1754 K, anisotropy is 0.06, figure 1 shows the simulation results of growth process of multiple grains in non-isothermal solidification. In the early stage of the growth, the grains are spherical. In time, due to the effect of anisotropy, the morphology of the grains changes from star-like to dendrite shape; by the end, the morphology of the grains had become complex as austenite dendrite (Figs. 1(a)–1(d)). In Fig. 1(b) the white lines on grains A, B, and C are projections of the normal to the $\{111\}$ plane of austenite grains onto the simulation region. In Figs. 1(b) and 1(c), the black lines on grains A, B, C, D, and E are parallel to the optimal growth direction ($\langle 100\rangle$) of the grains. The angle between two black lines is the angle between two optimal grain growth directions, and is equal to that of the normals to the $\{111\}$ plane and equal to that made by the $\{111\}$ planes therewith. For example, the angle between the optimal growth directions of grain A and grain B is the angle between the $\{111\}$ planes of the two grains. Here, this is defined as φ_{AB}. Also, φ_{AE}, φ_{AC}, φ_{BD}, and φ_{DE} are similar to φ_{AB}. Angle φ_{AC} (the angle between the $\langle 100\rangle$ directions of grain A and grain C), φ_{BD} (the angle between the $\langle 100\rangle$ directions of grain B and grain D), and φ_{DE} (the angle between the $\langle 100\rangle$ directions of grain D and grain E) are very small, so they are considered negligible here. In the simulation experiment, φ_{AB} and φ_{AE} are larger angles, while φ_{AC}, φ_{DE}, and φ_{BD} are smaller, so the grain boundaries between grains A and B, as well as those between A and E are large-angle grain boundaries, while those between A and C, D and E, and B and D are small-angle grain boundaries.

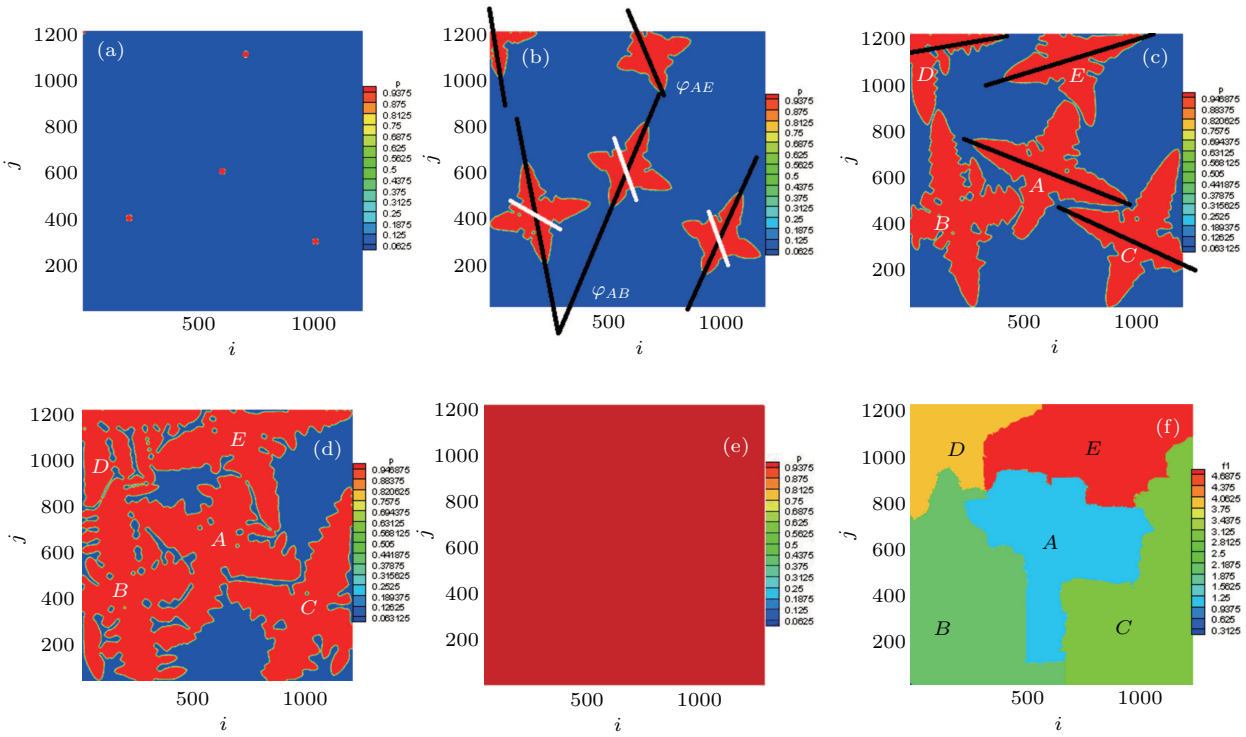


Fig. 1. (color online) Simulation of the growth morphology of multiple grains for (a) $t = 0\Delta t_1$, (b) $t = 3000\Delta t_1$, (c) $t = 6000\Delta t_1$, (d) $t = 12,000\Delta t_1$, (e) $t = 5 \times 10^5 \Delta t_1$, (f) grain boundary morphology.

With the growth of grains, the whole simulation region is gradually filled with austenite, as shown in Fig. 1(e). At this time, the Φ-value of the whole simulation area is 1 (where 1 represents the case where all of the simulated area is in a solid state). Grain boundaries cannot be observed in the phase field map when the simulation area is filled with austenite, therefore the grain boundary morphology, as shown in Fig. 1(f) which illustrates the grain orientation field corresponding to Fig. 1(e), was used. The figure describes various austenitic grain boundaries in Fig. 1(e). By denoting different grains with dissimilar colours, the shape and boundary of the grains are distinguished. It is convenient to study the nucleate position and its influence on the growth morphology of ferrite.

Figure 2 shows the distribution of solute at corresponding times to those in Fig. 1. It can be seen that the dendrite interface preface is the brightest, which suggests the highest solute concentration. Due to the redistribution of solute, the solute is enriched at the solidification interface preface. In addition, the solute is found at a high concentration between the secondary and tertiary dendrite arms.

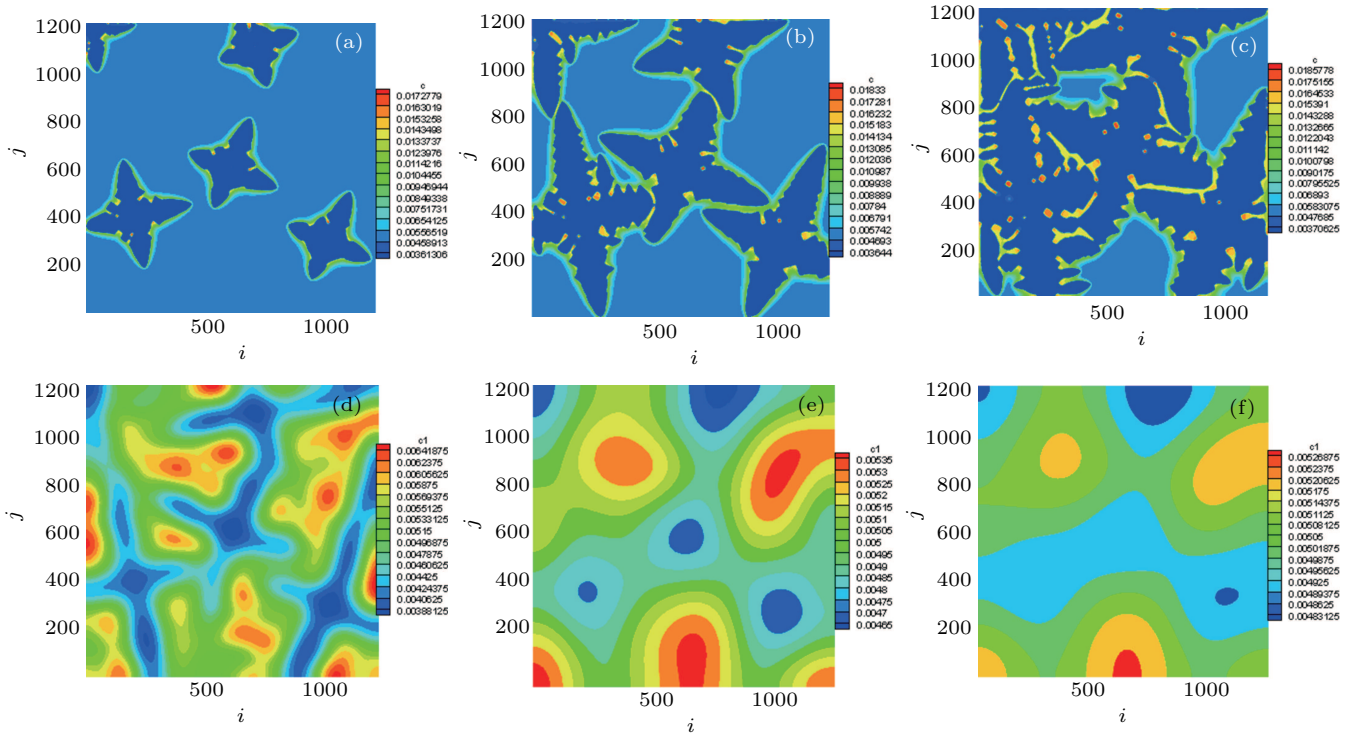


Fig. 2. (color online) Distribution of solute in the growth of multiple grains for (a) $t = 3000\Delta t_1$, (b) $t = 6000\Delta t_1$, (c) $t = 1.2 \times 10^4 \Delta t_1$, (d) $5 \times 10^5 \Delta t_1$, (e) $5 \times 10^8 \Delta t_{11}$, (f) $5 \times 10^9 \Delta t_{11}$.

Figure 2(d) shows the solute distribution corresponding to Fig. 1(e). It can be seen that, when the whole simulation area is filled with austenite, the solute still gathers near the grain boundaries, showing an uneven distribution. The simulation region did not reach the conditions (temperature, critical nuclear energy, and solute concentration) required for ferrite nucleation. In time, the temperature gradually decreases and the solute became uniformly diffused, which enabled ferrite nucleation. After the entire simulation area was filled with austenite, if the solute diffusion was simulated in accordance with the original time step, it would require a significant amount of computational effort; to facilitate simulation while reducing the calculation time, the method proposed in Subsection 3.3, using an enlarged time step Δt_{11} was used in the simulation region filled with austenite, so as to simulate the diffusion of both solute and temperature. That is to say, the diffusion of solute in the whole region is simulated by using the control equation for solute diffusion of Fick's law while keeping the morphology of the austenite unchanged, so that the solute in the austenite can spread faster and more uniformly while using a larger time step. The results are shown in Figs. 2(e)–2(f).

The multi-phase-field model in the study is a sequence function controlled by temperature: the temperature is the key to simulating the continuous evolution of microstructure in multiple phase transformations. The temperature gradient is not linear during phase transformation. However, in the simulation, due to the small simulation area, it is considered that the temperature gradient is linear in the simulation region. As the cooling rate is generally 10^{-1} K/s to 10 K/s orders of magnitude during solidification of medium and small castings at normal speeds,[29] a temperature gradient of 5 K/mm and a cooling rate of 5 K/s at the boundaries were added to the model. It is speculated that the heat is transferred from the bottom

up. As can be seen from Fig. 3 (the calculation conditions are the same as Fig. 1), the simulation results show that the temperature of the solidified area is higher than the area which is not solidified, and the solidification interface preface constantly releases latent heat. Similar to solute diffusion, when the whole simulation area is filled with austenite, based on the Fourier conduction equation, simulating the temperature changes at an enlarged time step Δt_{11} accelerates the calculation of temperature drop in the temperature field. As a result, the temperature conditions for ferrite nucleation are achieved faster. After a certain time, the heat transfer in the temperature field tends to be stable, when the temperature of the whole simulation area is close to the phase transformation temperature, as shown in Fig. 3(d). The temperature difference of the simulation area is caused by the added temperature gradient and cooling rate at the boundaries.

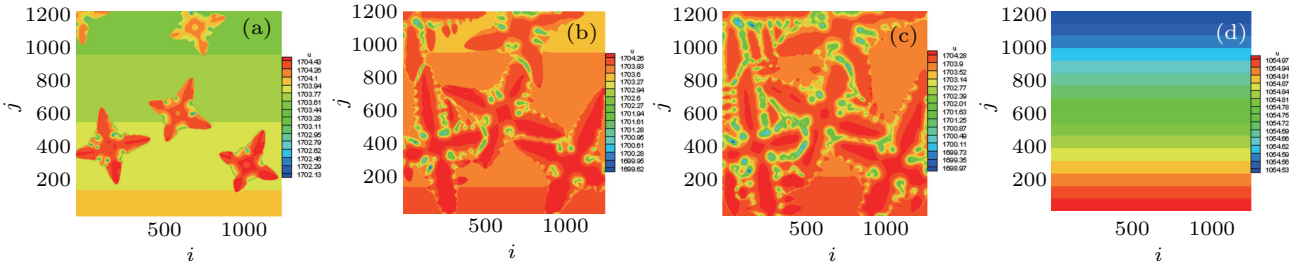


Fig. 3. (color online) Simulation of temperature variation in a non-isothermal phase field for (a) $t = 3000\Delta t_1$, (b) $t = 6000\Delta t_1$, (c) $t = 1.2 \times 10^4 \Delta t_1$, (d) $5 \times 10^{11} \Delta t_{11}$.

4.2. Solid-state phase transformation

With the decrease in the temperature of the simulated region, ferrite begins to nucleate when the temperature (1048 K) decreases to that at which austenite is transformed to ferrite. The ferrite nucleation sites are dictated by the free energy of the whole simulation region, and the density of nucleation sites is governed by Eq. (15). The simulation results of solid-state phase transformation are shown in Fig. 4. It can be seen from Fig. 4(a) that ferrite nucleates at austenite grain boundaries. This is because, as the temperature drops, the interface structure becomes loose, that is, the phase angle increases at the grain boundaries. This lowers the energy barriers (activation energy) which need to be overcome by atoms in the parent phase to enter new phases after crossing the interface through thermal activation. At the same time, the average distance moved by each atom is reduced due to the increasing number of defects. There is a higher critical nucleation energy seen at grain boundaries, which make it easy for nucleation to occur. The nucleation phenomenon in Fig. 4(a) is consistent with the nucleation theory of Cahn.[30] Figures 4(b)–4(d) show the growth in ferrite nucleation. It can be seen that grains nucleate at grain boundaries and different nucleation sites have different morphologies. Due to the anisotropic effect, different ferrites grow at different rates in different directions, that is, grains have different growth rates in different parent phases. In Fig. 4(c), grain H grows faster in the parent austenite (grain B) than in grain A, because the habit plane of ferrite grain H is the austenite grain plane (111). The existence of the habit plane means that the new phase ferrite, which shows a good lattice match to its mother phase austenite, grows faster. This is similar to grains such as I, J, K, and L, and the phenomenon is consistent with the K-S relationship.[27]

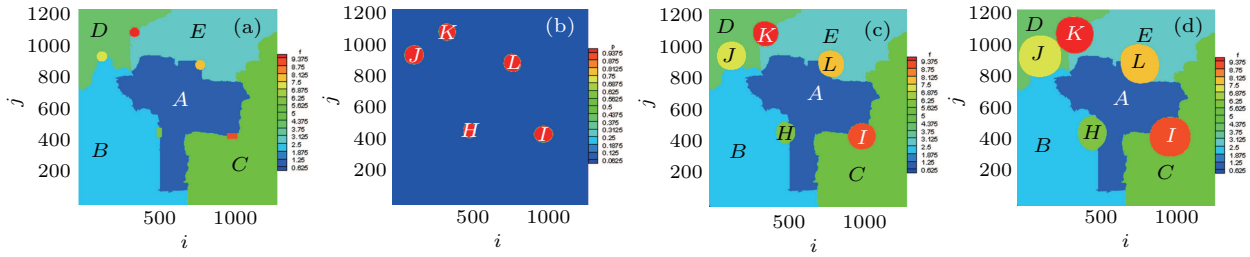


Fig. 4. (color online) Simulation of the growth of ferrite grains for (a) $1000\Delta t_2$, (b) $5000\Delta t_2$, (c) $1 \times 10^4 \Delta t_2$, (d) $2 \times 10^4 \Delta t_2$.

The orientation field of grains affects the interfacial energy, while the growth rate of grains is controlled by the interfacial energy. Grain I in Fig. 4(d) grows faster than grain H, because the angle between the austenite grains A and B is larger than that between grains A and C (Fig. 1(b)), that is, grain I has a better lattice match with its parent phase. Thus, it was concluded that the smaller the angle between austenite grains, the faster the rate of growth rate of ferrite grains in this nucleation scenario. According to the theory of phase transformation, the transformation always tries to consume less energy, so ferrite always grows along the direction consuming the least energy, which is parallel to the close-packed plane

of atoms with a low index. It helps to reduce the interfacial energy thereat. The grid number occupied by grains is used to express the growth of ferrite grains, as shown in Fig. 5, in which the slope of the curve represents the growth rate of grains. For examples, the black and the red lines represent the growth of grains H and I. It can be seen that curve I inclines more obviously than curve H, that is to say, the growth rate of grain I is greater than that of the grain H. To analyze this phenomenon from the perspective of crystallography, the phenomenon characterized by the simulation results accords with the theory dictating that grain boundaries affect the γ–α phase transformation.[32–34]

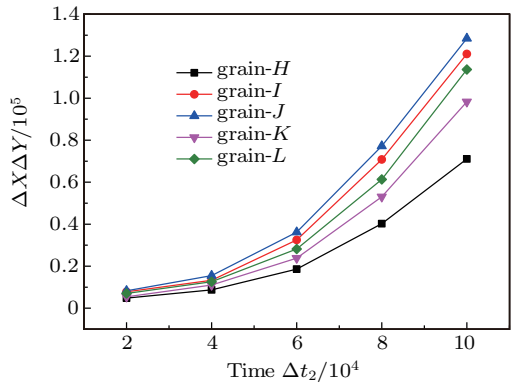


Fig. 5. (color online) Rates of growth of ferrite grains.

Grain I in parent grains A and C shows a smaller difference in growth rate than grain H in parent grains A and B, as shown in Fig. 4(d). This is because the angle φ_{AB} between the austenite grains A and B is greater than that between grains A and C (φ_{AC}). The difference of the rate of growth of ferrite in different parent phase grains that nucleates at large-angle austenite grain boundaries on both sides of the boundaries is greater than that at small-angle austenite grain boundaries: this can be explained by the grain growth relationship K-S[27] and the theory governing boundaries affecting the γ–α phase transformation kinetics.[32–34]

Figure 6 shows the distributions of solute corresponding to Fig. 4 (different color scales in the figure represent different concentrations). It may be seen that the over-saturated carbon atoms dissolved from the ferrite phase are transferred to the austenite phase, and contribute to carbon enrichment at the ferrite–austenite interface. With a continuously increasing carbon concentration, a concentration gradient of carbon atoms is formed on one side of the austenite. Driven by this concentration gradient, the ferrite becomes coarsened through carbon diffusion and transformation of grain structures. Figure 6(d) shows that the carbon concentration at grain boundaries is the highest when grains J and K meet. With the growth of ferrite, the carbon transfers, and contributes, to a uniform concentration thereof in the side containing the austenite phase.

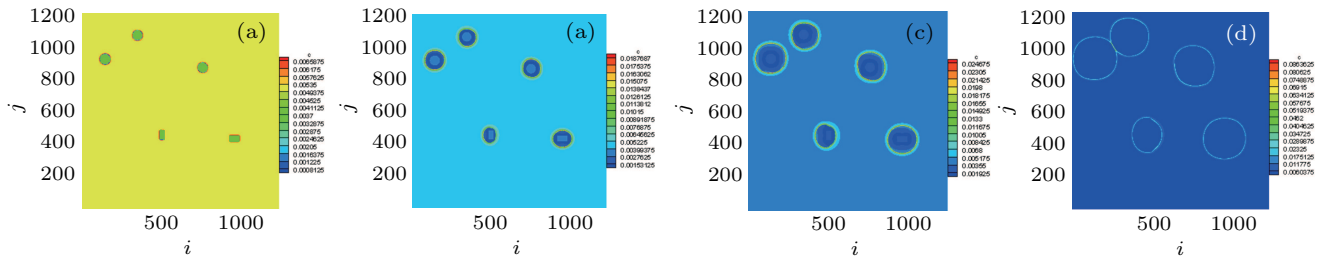


Fig. 6. (color online) Distribution of solute in ferrite grains for (a) $1000\Delta t_2$, (b) $5000\Delta t_2$, (c) $1\times10^4\Delta t_2$, (d) $2\times10^4\Delta t_2$.

5. Conclusions

This research establishes the sequence function with temperature as its independent variable, and a new multi-phase-field model for liquid–solid–solid multi-phase transformation by coupling the liquid–solid phase transition model with the solid–solid phase transition model. Taking an Fe–C alloy as an example, the continuous evolution of a multi-phase transformation is simulated.

Ferrite grains, which nucleate at the boundaries of the austenite grains, grow at different rates in parent austenite grains with different orientations. The ferrite grains nucleating at small-angle austenite grain boundaries have a greater rate of growth than those nucleating at large-angle austenite grain boundaries. The difference of the growth rate of ferrite grains in different parent phases that nucleate at large-angle austenite grain boundaries on both sides of the boundaries is larger than that of grains nucleating at small-angle austenite grain boundaries.

While being transformed from austenite to ferrite, the over-saturated carbon atoms transit to the austenite phase, and this therefore results in carbon enrichment at the ferrite–austenite interface.

References

[1] Luo Z R 2013 "Phase Field Modeling of Microstructure Evolution in Metallic Materials," Ph. D. Thesis (Nanning: Guangxi University) (in Chinese)

[2] Boussinot G, Finel A and Le B Y 2009 *Acta Mater.* **57** 921

[3] Wang J, Li X K, Liu C and Shi Y N 2016 *Acta Mechanica Solida Sinica* **37** 1 (in Chinese)

[4] Raabe D 2002 *Computational Materials Science* (Beijing: Beijing Chemical Industry Press) p. 223

[5] Sun R X 2010 "Simulation for the austenite to ferrite transformation", MS Thesis (Kaifeng: Henan University of Technology) (in Chinese)
[6] Bottger B, Schmitz G J and Santillana B 2012 *Trans. Indian Inst. Met.* **65** 613
[7] Zhao D P, Jing T and Liu B C 2003 *Acta Phys. Sin.* **52** 1737 (in Chinese)
[8] Feng L, Wang Z P, Lu Y and Zhu C S 2008 *Acta Phys. Sin.* **57** 1084 (in Chinese)
[9] Feng L, Wang Z P, Zhu C S and Lu Y 2009 *Chin. Phys. B* **18** 1985
[10] Niu Y E 2008 "Phase-Field Simulation of Fe–C Alloy in the Isothermal Solidification," MS Thesis (Xi'an: Xi'an Technological University) (in Chinese)
[11] Heo T W and Chen L Q 2014 *The Minerals, Metals & Materials Society* **66** 1520
[12] Bradley J R, Rigsbee J M and Aaronson H I 1977 *Metall. Trans. A* **8A** 323
[13] Mecozzi M G, Militzer M, Sietsma J and van der Zwaag S 2008 *Metallurgical and Materials Transactions A* **39** 1237
[14] Huang C J, Browne J D and McFadden S 2006 *Acta Mater.* **54** 11
[15] Loginova I, Odqvist J, Amberg G and Agren J 2003 *Acta Mater.* **51** 1327
[16] Mecozzi M G, Militzer M, Sietsma J and van der Zwaag S 2006 *Acta Mater.* **54** 3691
[17] Mecozzi M G, Sietsma J and van der Zwaag 2006 *Acta Mater.* **54** 1431
[18] Pariser G, Schaffnit P, Steinbach I and Bleck W 2001 *Stell. Res.* **72** 354
[19] Bhattacharya A, Upadhyay C S and Sangal S 2015 *Metallurgical and Materials Transactions A* **64** 926
[20] Mecozzi M G, Sietsma J and van der Zwaag 2005 *Comput. Mater. Sci.* **34** 290
[21] Huang C J and Browne J D 2006 *Metallurgical and Materials Transactions A* **37** 589
[22] Song S T 2008 "A Phase-field Simulation of Austenite to Ferrite Transformation in Low Carbon Steels," MS Thesis (Jinan: Shandong University) (in Chinese)
[23] Yeddu H K, Borgenstam A and Ågren J 2013 *J. Alloys Compd.* **577** 141
[24] Chang K and Moelans N 2014 *Acta Mater.* **64** 443
[25] Kim S G, Kim W T and Suzuki T 2004 *J. Crystal Growth* **261** 135
[26] Feng L, Jia B B, Zhu C S, Lu Y, Xiao R Z and Feng X J 2016 4*th International Conference on Sensors*, December 27–28, 2016, Shenzhen, China, p. 855
[27] Cheng X N, Dai Q X and Shao H H 2006 *Solid phase transformation and diffusion of materials* (Beijing: Chemical Industry Press) pp. 57–70
[28] Steinbach I and Apel M 2006 *Physica D* **217** 153
[29] Xiao R Z, An G S, Zhu C S, Wang Z P and Yang S Y 2014 *Transactions of Nonferrous Metals Society of China* **24** 3639
[30] Cahn J W 1956 *Acta Metal* **4** 458
[31] Cai D 2012 "Simulation of the influence of interfacial snisotropic on the microstructure evolution by phase-field approach", MS Thesis (Changsha: Central South University) (in Chinese)
[32] Jiang Y H 2014 "Application of analytical model for the study of interface-controlled solid-state phase transformation kinetics", Ph. D. Thesis (Xi'an: Northwestern Polytechnical University) (in Chinese)
[33] Zhang L F and Liu Y C 2012 *Heat Treatment of Metals* **37** 29
[34] Wu H D, Zhang C, Liu W B and Yang Z G 2015 *Acta Metal. Sin.* **51** 1136